The Astrophysical Journal Letters, 898:L13 (6pp), 2020 July 20 https://doi.org/10.3847/2041-8213/aba266

Erosion-driven Size Redistribution of Protoplanetary Disk Solids and the Onset of Streaming Instability and Pebble Accretion

Evgeni Grishin, Mor Rozner, and Hagai B. Perets
Technion, Israel Institute of Technology, Haifa 3200003, Israel; eugeneg@campus.technion.ac.il
Received 2020 April 7; revised 2020 June 24; accepted 2020 July 2; published 2020 July 20

Abstract

The formation of the first planetesimals and the final growth of planetary cores relies on the abundance of small pebbles. The efficiencies of both the streaming instability (SI) process, suggested to catalyze the early growth of planetesimals, and the pebble-accretion process, suggested to accelerate the growth of planetary cores, depend on the sizes of solids residing in the disk. In particular, these processes were found to be sensitive to size distribution of solids, and efficient planetesimal formation and growth through these channels require a limited pebble size distribution. Here we show that aeolian erosion, a process that efficiently grinds down boulders into a mono-sized distribution of pebbles, provides a natural upper limit for the maximal pebble sizes (in terms of their Stokes number). We find the dependence of this upper limit on the radial separation, disk age, turbulence strength, and the grain-size composition of the boulders in the disk. SI is favorable in areas with a Stokes number less than 0.1, which is found in the inner sub-astronomical-unit regions of the disk. This upper limit shapes the size distribution of small pebbles and thereby catalyzes the early onset of planetesimal formation due to SI, and the later core accretion growth through pebble accretion.

Unified Astronomy Thesaurus concepts: Planet formation (1241); Protoplanetary disks (1300); Planetesimals (1259)

1. Introduction

The early stages of planet formation occur in protoplanetary disks around young stars, which initially contain mostly gas and roughly 1% of dust. Planet formation takes place over many orders of magnitude, beginning with micron-sized dust grains, which collisionally grow to centimeter-sized pebbles and later grow into kilometer-sized planetesimals, and eventually form planetary embryos and planets (Chiang & Youdin 2010).

Although the early growth of dust grains can be understood through collisional processes, the formation of the first planetesimals proves to be a major challenge. Small grains are tightly coupled to the gas flow and can efficiently grow to millimeter–centimeter pebbles. The larger meter-sized boulders are partially decoupled from the gas flow and experience various growth barriers (Blum & Wurm 2008, and references therein). In particular, the radial-drift barrier prevents particles from growing beyond centimeter–meter scales, since such boulders are effectively lost to the main star (Adachi et al. 1976; Weidenschilling 1977), and collisional fragmentation limits rapid growth of ∼meter-size boulders (Blum & Wurm 2008). Interstellar planetesimal seeding (Grishin et al. 2019) could provide large enough planetesimals to young systems, thus liberating them from their initial growth barriers. The generation of the first planetesimals, however, is still debated.

Recently, we suggested that aeolian-erosion gives rise to an additional potential growth barrier for pebble/boulder/rock growth, where beyond a certain threshold velocity, the headwind from the gas flow erodes material from the surface of the boulder, as it overcomes the cohesive forces holding its material together (Rozner et al. 2020). The erosion can either grind down larger boulders into smaller pebbles, or set an additional growth barrier for the growing pebbles, even if the other barriers are circumvented.

The streaming instability (SI; Youdin & Goodman 2005) is a potentially promising mechanism to overcome the radial drift (and other barriers) to form planetesimals. SI catalyzes the localized concentration of solids in the disk to the point where gravitational collapse can operate and directly form large planetesimals. Possible observations and simulations that support this channel rely on studies of asteroid size distributions (Morbidelli et al. 2009; Li et al. 2019) and binary Kuiper Belt object binary masses, compositions (Nesvorný et al. 2010), and orientations (Nesvorný et al. 2019). However, the robustness of SI is debated. In particular, SI that leads to the production of strong clumping and successful planetesimal formation requires large metallicity in the protoplanetary disk, a local dust to gas ratio above unity, and an optimal size of the pebbles and pressure gradients (Johansen et al. 2009b; Yang et al. 2017; Sekiya & Onishi 2018).

Early SI studies assumed simple mono-size distribution of solids in the disk. However, recently, Krapp et al. (2019) showed that SI proves to be far less efficient when multisize solid distribution is considered. They find that for a sufficiently wide distribution of pebble sizes, the timescale for the growth of the SI unstable mode is linearly decreasing with the number of species and does not converge (see Figures 2 and 4 of Krapp et al. 2019). Interferometric and scattered light observations of young disks suggest the coexistence of both small μ-sized grains and ∼centimeter-sized pebbles (Menu et al. 2014; van Boekel et al. 2017). Thus, the existence of a wide size distribution, typically expected in planet formation models (Bai & Stone 2010; Schaffer et al. 2018) could severely limit the applicability of the SI scenario.

At later stages, the formation of gas/ice giants requires the growth of planetary cores in the standard core accretion scenario (Pollack et al. 1996). The source of the accreted solids was first attributed to planetesimals, but the accretion rate was found to be too slow to efficiently grow planetary cores at large

separations. However, it was later suggested that wind-assisted accretion of pebbles could provide a more efficient channel for planetary accretion and growth (Ormel & Klahr 2010; Perets & Murray-Clay 2011; Lambrechts & Johansen 2012). The growth rate and hence the final embryo/planet mass depend on many parameters, including the pebble sizes and abundance, the location in the disk, core formation times (Bitsch et al. 2015; Visser & Ormel 2016; Ormel & Liu 2018), turbulence levels (Rosenthal & Murray-Clay 2018, 2019), and planetary envelope structure and evolution (Lambrechts & Lega 2017; Brouwers et al. 2018).

Both the early planetesimal formation via SI and later subsequent formation of planets due to core accretion rely on the flow of pebbles. Only pebbles of a certain size range, pending the disk model and radial location, can significantly contribute. Thus, the concentration of pebbles of similar sizes in a localized region in the disk could be beneficial for the formation and growth of planetesimals/planets (Liu et al. 2019).

Various mechanisms for concentration of particles have been suggested, including vortices (Barge & Sommeria 1995; Raettig et al. 2015), zonal flows (Johansen et al. 2009a), pressure bumps (Pinilla et al. 2012; Zhu et al. 2012) or planetary torques (Benítez-Llambay & Pessah 2018; Chen & Lin 2018). These mechanisms involve either complex turbulent magnetohydrodynamical effects and/or preexisting planets and have been studied mostly numerically. Here we present a simple, analytic model for the redistribution of disk solid sizes due to a different mechanism, namely aeolian-erosion.

In this Letter we utilize the aeolian-erosion barrier as a natural source of size-segregation and concentration. We focus on the first stages of planet formation assuming no planets or pressure bumps are present. We consider laminar disk flow, and later discuss turbulent disks. In Section 2 we review the aeolian-erosion mechanism and derive the upper limit for the critical Stokes number of surviving solids as a function of the radial location on the disk and the size of the detached grains (i.e., assuming pebbles/boulders are composed of small grains of some typical size, which are removed by the head winds) for laminar and turbulent flows. This, in turn, effectively determines the maximal size of eroded pebbles that survive in the disk. We discuss the implications of the aeolian-erosion pebble size-limit for the SI and pebble accretion processes in Section 3 and summarize in Section 4.

2. Critical Stokes Number from Aeolian Erosion

2.1. Aeolian Erosion

In Rozner et al. (2020), we introduced and discussed the concept of the aeolian-erosion barrier. As small pebbles grow into boulders they are held by cohesive forces. The wind from the gas flow can detach dust grains and pebbles from the surface of the growing boulder. The threshold relative wind velocity at the point when the shear pressure overcomes the cohesion and detaches the particle from the boulder surface is derived from Shao & Lu (2000)

$$v_{\rm th} = \sqrt{\frac{A_N \gamma}{\rho_g d}}, \tag{1}$$

where ρ_g is the local gas density and d is the typical size of the grains composing the pebble. A_N is a dimensionless number that depends on the Reynolds number, and γ is the surface energy. Wind tunnel experiments found a good fit with a constant value of $A_N = 1.23 \times 10^{-2}$ and γ in the range of $(1.65–5) \times 10^{-1}$ g s^{-2} for grain sizes in the range of 50–1800 μm (Iversen & White 1982). Recent microgravity experiments of silicate glass spheres measured the surface energy in the range of $\gamma = 7.8 \pm 3.8 \times 10^{-2}$ g s^{-2} (Demirci et al. 2020). We choose $\gamma = 1.65 \times 10^{-1}$ g s^{-2} to be compatible with both experiments.

When the relative velocity exceeds the threshold velocity, grains from the outer layer of the pebble/boulder are removed and the mass loss rate is fast. The erosion timescale is (Rozner et al. 2020).

$$t_{\rm ero} = \frac{R}{|\dot{R}|} = \frac{4\pi R^2 \rho_p F_{\rm coh}}{\rho_g v_{\rm rel}^3 m_d}, \tag{2}$$

where R is the size of the body, $v_{\rm rel}$ is the relative velocity, $F_{\rm coh}$ is the strength of the cohesive forces and m_d is the mass of the released grains. The cohesive force scales as $F_{\rm coh} \propto d$, the grain size, with a proportionality constant around 10^2 g s^{-2}, determined from experiments (see Rozner et al. 2020 and Shao & Lu 2000 for details and references.) Generally, the erosion will be very fast, comparable to dynamical timescales for particles less than $\lesssim$10 m (see, e.g., Figure 2 of Rozner et al. 2020), which is comparable to the rapid erosion rates determined in wind tunnel experiments of Paraskov et al. (2006), and more recent microgravity experiments of Demirci et al. (2020). The mass loss continues until the relative wind velocity (which changes due to the continuous decrease in the size of the eroding pebble) becomes smaller than the threshold velocity.

The gas flows in a sub-Keplerian velocity determined by the pressure gradient profile and the location in the disk. The deviation from Keplerian velocity is measured by $\eta \propto (h/a)^2$, where h is the scale height and a is the distance from the star. Using polar coordinates, the components of relative velocity between the object and gas are (we generally follow the same disk model as assumed in Perets & Murray-Clay 2011 and references therein)

$$\begin{aligned} v_{\rm rel,r} &= -\frac{2\eta v_k \tau_s}{1+\tau_s^2},\ v_{{\rm rel},\phi} \\ &= -\eta v_k \left(\frac{1}{1+\tau_s^2} - 1\right), \end{aligned} \tag{3}$$

where the Stokes number is defined by

$$\tau_s = \Omega t_{\rm stop};\ t_{\rm stop} = \frac{m v_{\rm rel}}{F_D}, \tag{4}$$

where Ω is the angular Keplerian velocity, v_k is the Keplerian velocity, m is the object's mass, and $t_{\rm stop}$ is the stopping time. F_D is the aerodynamic drag force.

In Figure 1 we show the aeolian-erosion time evolution of bodies of various initial sizes, but using the Stokes number as a measure. In obtaining Figure 1 we used the flared Chiang–Goldreich disk model (Chiang & Goldreich 1997, see also Perets & Murray-Clay 2011 and Grishin & Perets 2015), with $\eta \approx 2 \times 10^{-3}(a/{\rm au})^{4/7}$ and $\rho_g = 3 \times 10^{-9}(a/{\rm au})^{-16/7}$ g cm^2. We used $a = 1$ au and $d = 0.1$ cm, similarly to our default assumption in Rozner et al. (2020). The final Stokes number

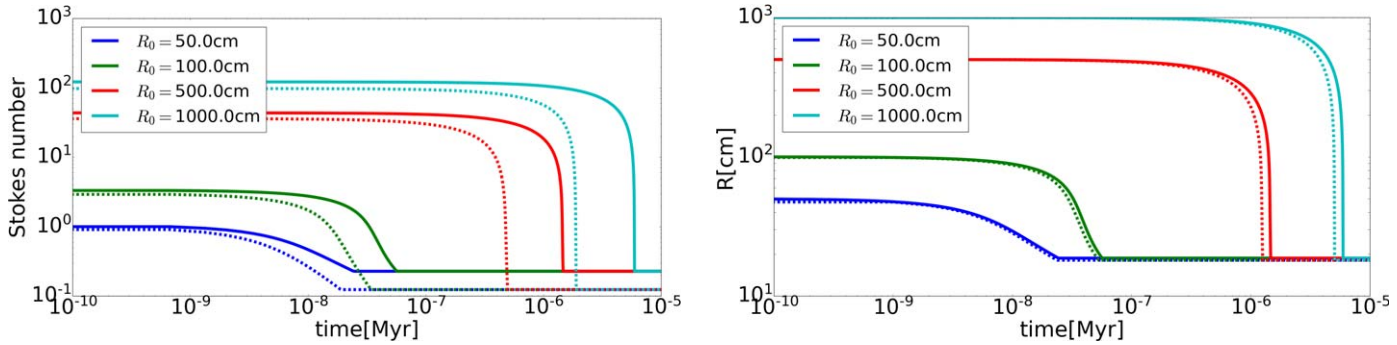

Figure 1. Time-evolution of the Stokes number (left) and of the body size (right) on the initial size of the body at a fixed distance of $a = 1$ au from the star, and dust grains of size $d = 0.1$ cm. Solid lines correspond to integration with the laminar relative velocity. Dashed lines depict integration of both laminar and turbulent velocity.

will lower for the case of turbulent velocities, as explained below.

2.2. Critical Stokes Number

The conclusion from Figure 1 is that the size distribution of particles is limited to a critical Stokes number, $\tau_\star$, which depends on the properties of the composing grains, the sizes of the eroding pebbles and the properties of the disk. For only laminar relative velocities, we present an analytic solution for $\tau_\star$ as a function of the grain and disk properties. For the turbulent case, we arrive at a fifth-order polynomial and find its roots numerically. We discuss the implications for SI later in Section 3.

2.2.1. Laminar Case

The scalar relative velocity from Equation (3) is

$$v_{\rm rel} = \sqrt{v_r^2 + v_\phi^2} = \eta v_K \frac{\tau_s\sqrt{4+\tau_s^2}}{1+\tau_s^2} \equiv \eta v_k g(\tau_s). \tag{5}$$

The erosion is quenched once $v_{\rm rel}(\tau_s) \leqslant v_{\rm th}$, which defines the critical Stokes number $\tau_\star$ as a function of the radial location on the disk. By setting the dimensionless laminar relative velocity $\kappa_{\rm l} \equiv \eta v_k / v_{\rm th}$ the condition becomes $g(\tau_\star) = \kappa_{\rm l}^{-1}$. Inverting the equation leads to a second degree polynomial, solved via the standard quadratic formula to yield

$$\tau_\star = \left[\frac{1 - 2\kappa_{\rm l}^2 + \kappa_{\rm l}\sqrt{4\kappa_{\rm l}^2 - 3}}{\kappa_{\rm l}^2 - 1}\right]^{1/2}. \tag{6}$$

The existence of a real solution requires $\kappa_{\rm l} \geqslant \sqrt{3}/2$. Note that the case $a = 1$ au and $d = 0.1$ cm leads to $\tau_\star \approx 0.22$, which is the critical Stokes number in our example in Figure 1.

2.2.2. Turbulent Case

The disk could also be turbulent. The strength of the turbulence is parameterized by the standard Shakura–Sunyaev parameter α. The relative turbulent velocity depends on α and on the dimensionless Stokes and turbulent Reynolds numbers. The turbulent Reynolds number is the ratio of the turbulent to molecular viscosity or the ratio of the largest eddy to the mean free path (Rosenthal et al. 2018). In any case, the turbulent Reynolds number is of the order $\sim\alpha \times 10^{10}$ and much larger than any typical Stokes number.

In the limit of infinite turbulent Reynolds number, the turbulent velocity component is given by $v_{\rm turb} = \sqrt{\alpha} c_s \sqrt{\tau_s/(1+\tau_s)}$, where the sound speed is $c_s \approx 6.6 \times 10^4 (a/{\rm au})^{-3/14}$ cm s^{-1}. Note that the ratio $c_s/v_k \approx 0.022(a/{\rm au})^{2/7}$ is the aspect ratio of the disk, as set from the disk profile. The total relative velocity is the sum of the squares of the laminar and turbulent velocities, $v_{\rm tot}^2 = v_{\rm rel}^2 + v_{\rm turb}^2$.

The erosion stops once $v_{\rm tot} \leqslant v_{\rm th}$. Similarly to the laminar case, we can define the dimensionless turbulent velocity $\kappa_{\rm turb} \equiv \sqrt{\alpha} c_s / v_{\rm th}$, and the condition for the critical Stokes number becomes:

$$\kappa_{\rm l}^2 \frac{\tau_\star^2(4+\tau_\star^2)}{(1+\tau_\star^2)^2} + \kappa_{\rm turb}^2 \frac{\tau_\star}{1+\tau_\star} = 1. \tag{7}$$

After some algebra, Equation (7) can be rewritten as a fifth-order polynomial in $\tau_\star$:

$$\begin{aligned} p(\tau_\star) = &(\kappa_{\rm l}^2 + \kappa_{\rm turb}^2 - 1)\tau_\star^5 + (4\kappa_{\rm l}^2 + 2\kappa_{\rm turb}^2 - 2)\tau_\star^3 \\ &+ (\kappa_{\rm l}^2 - 1)\tau_\star^4 + (4\kappa_{\rm l}^2 - 2)\tau_\star^2 + (\kappa_{\rm turb}^2 - 1)\tau_\star - 1 \\ = &\ 0. \end{aligned} \tag{8}$$

Unfortunately, there is no explicit expression for the roots of a fifth-degree polynomial,[1] but the roots can be found numerically.

Figure 2 shows the critical Stokes number τ_s as a function of the orbital separation. Solid lines are the solution of Equation (6) with only laminar disk considered, while dashed lines are the solution to the turbulent disk, Equation (8) with $\alpha = 10^{-2}$. Equation (8) has been solved numerically using the `numpy.polynomial` module. The solution is the smallest positive real solution. Each line represents different grain size that determines the threshold velocity in Equation (1). Generally the critical Stokes number is a decreasing function on the radial separation. The larger the size of the pebbles, the farther in disk will erosion take place.

[1] Solutions to third- and forth-order polynomials by radicals were known already in the 16th century. The first attempts of a proof of no analytic formula for the fifth degree was presented by Paolo Ruffini (Ruffini 1799). His proof was incomplete and corrected by Niels Henrik Abel (Abel 1824). This is known as the Abel–Ruffini theorem. Later, it was superseded by what is known today as Galois' theory (Galois 1846), which was published postmortem only in 1846, 14 yr after the tragic death of Évariste Galois at 1832.

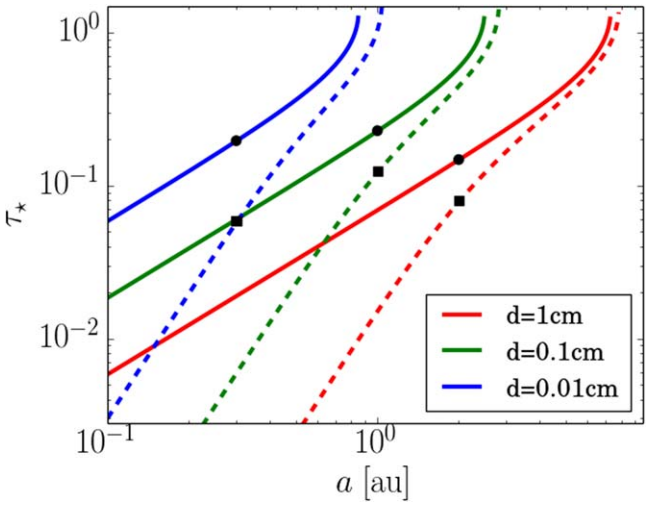

Figure 2. Critical Stokes number $\tau_\star$ as a function of the orbital separation a. Each line is the solution to Equation (8). Solid lines are solutions of the laminar velocity only ($\kappa_t \equiv 0$ in Equation (8)). Dashed lines are the solution with both laminar and turbulent velocity, with the α-viscosity equals to $\alpha = 0.01$. Red (top), green (middle), and blue (bottom) lines correspond to detaching grain sizes of 1, 0.1, 0.01 cm, respectively. Black circles indicate numerical integration of the erosion equation with laminar velocities for $a = 0.3$, 1, 2 au and $d = 0.01$, 0.1, 1 cm, respectively. Black squares indicate the same numerical integration, but with both laminar and turbulent velocities.

2.3. Disk Structure and Evolution

The calculation of the critical Stokes number was done under the assumption of a minimal mass solar nebula (MMSN; Hayashi 1981; Perets & Murray-Clay 2011) background gas density. In reality, disk profiles could vary in shape and slope (Raymond & Cossou 2014), and the gas density may vary due to various global and local effects. Transitional disks of depleted gas density are favorable for the formation of super-Earths (Lee & Chiang 2016), and the formation of ice giants requires the core to form relatively late in order to avoid runaway gas accretion (Bitsch et al. 2015). SI was considered and found to be more efficient following disk evolution in depleted disks, where the metallicity is artificially enhanced (Carrera et al. 2017).

Here we focus on the global disk dissipation and do not discuss local and/or transient effects, which could potentially be important, but are beyond the scope of the current study. We demonstrate the dependence on the results on the different gas densities.

Observations of young clusters show that protoplanetary disks live only a few megayears and could be fitted with exponential time dependence (Mamajek 2009). We assume for simplicity that the gas density follows an exponential decay law, $\rho_g(t) = \rho_g(0)\exp(-t/\tau_{\rm disk})$, where $\tau_{\rm disk} \approx 3$ Myr. Since $v_{\rm th} \propto \rho_g^{-1/2}$, the dimensionless parameter $\kappa_{\rm l}$ will decrease until the erosion stops. For laminar velocity, the critical Stokes number depends on time via $\kappa_{\rm l}$, which will approach $\sqrt{3}/2$ at a finite erosion-stopping time

$$t_{\rm es} = \tau_{\rm disk} \ln \frac{4 d \rho_0 \eta^2 v_K^2}{3 A_N \gamma}. \quad (9)$$

At this time, the critical Stokes number will increase up to a limiting value of $\tau_\star(\kappa_{\rm l} \to \sqrt{3}/2^+) = \sqrt{2} \approx 1.414$. For our fiducial values of $d = 0.1$ cm at 1 au, the erosion-stopping time is $t_{\rm es} \approx 1.96\tau_{\rm disk} \approx 5.9$ Myr. The result sensitively depends on the location in the disk. At larger radial locations $t_{\rm es}$ is reached faster since $\kappa_{\rm l}$ is smaller there, and vice versa.

For turbulent velocities, both $\kappa_{\rm l}$ and $\kappa_{\rm turb}$ will decrease with decreasing gas density. The critical Stokes number will increase, and generally larger Stokes numbers are possible. The erosion-stopping time is hard to compute analytically, but we expect it to be similar to the time obtained for the laminar case.

To summarize, the critical Stokes number increases with time as the disk is depleted. Therefore, assuming some supply rate $\dot{M}_{\rm supp}(t)$ of larger boulders and planetesimals (e.g., from pebbles drifting from larger separations where erosion was inefficient), the time-dependent erosion will leave traces of eroded material with a time-dependent critical Stokes number $\tau_\star(t)$. The rate of erosion of larger boulders leading to production of grains/pebbles by the aeolian-erosion is $dN(\tau_\star)/dt = \dot{M}_{\rm supp}(t)/m_d(\tau_\star) \propto \tau_\star^{-3}$, where $m_d(\tau_\star)$ is the mass of the grain at Stokes number $\tau_\star$. In principle, the production rate can be integrated to obtain the total number of new grains at a given time, but the integration is not trivial since both $\tau_\star$ and $\dot{M}_{\rm supp}(t)$ could have a complicated dependence on time. The number of new grains should decrease as the Stokes number increases.

3. Discussion and Implications

Size distributions: The initial size distribution of disk solids is usually considered to be following a power law with index q ($n(r) \propto r^{-q}$). Observations of interstellar dust indicate that $q = 3.3$–3.6 (Mathis et al. 1977). Evidence of multiple grain-size populations have also been detected in molecular clouds (Pagani et al. 2010; Andersen et al. 2013) and in protoplanetary disks (Banzatti et al. 2011; Jin et al. 2019). The actual formation channels for boulders beyond the drift and fragmentation barriers are debated. Various mechanisms have been suggested to overcome the growth barriers, such as local pressure maxima, particle pile-ups, rapid coagulation, etc. (see Section 4.3 in Armitage 2010 and references therein). Nevertheless, a large reservoir of $\tau_s \sim 1$ pebbles is the starting point of the pebble accretion paradigm, and the numerical SI study of Krapp et al. (2019) uses a wide range of sizes up to $\tau_s \sim 1$. The interstellar pebble and planetesimal reservoir could have been captured in most stages of the protoplanetary disk lifetime (Grishin et al. 2019), or at an earlier stage during the molecular cloud phase (Pfalzner & Bannister 2019), which would enrich the protoplanetary nebula with an abundance of pebbles and boulders. We remain agnostic to the exact mechanism that forms these boulders and assume that a large reservoir exists, similarly to the standard pebble accretion scenario and other studies that assume an initial size distribution (e.g., Krapp et al. 2019).

Regardless of the theoretical and observational uncertainties, the power law is expected to be steep. At $t = t_0$ the distribution is strictly a power law. As time progresses, dust will grow and the minimal size will increase. In addition, particles with $\tau_s > \tau_\star$ will be eroded to smaller pebbles with $\tau_\star$. If the growth is slow or inefficient, there will be little effect on the underlying distribution, since the total mass is dominated by the lighter dust particles. The only changes in the underlying power-law distribution are the boundaries of the minimal and maximal sizes, shaped by growth and erosion (and other barriers), respectively.

Nevertheless, the shaping of the dust size distribution could have an effect on a local scale. Since each radial separation a determines a typical Stokes number $\tau_\star(a)$, different locations will have different typical dust sizes, which could in turn serve as a ubiquitous mono-dispersed local population. This population can be important for the onset of other growth mechanisms as described below.

Streaming instability: Particles with $\tau_s > \tau_\star$ rapidly erode to $\tau_\star$ on dynamical timescales, much faster that the growth of SI. Thus, $\tau_\star$ is a natural upper limit for the allowed Stokes numbers for the initial multispecies size distribution. The inner parts of the disk will have lower $\tau_\star$. Although this natural upper limit is considered a barrier, it could actually help catalyze planet formation via SI.

Recently, Krapp et al. (2019) have provided the first systematic study of the linear growth of the multispecies SI. They varied the minimal and maximal ranges of the Stokes number, the number of species N and the local dust-to-gas density, ϵ, and studied the timescale for the growth of the most unstable mode in each case. The most striking conclusion is that the convergence was not achieved with increasing number of species. In particular, even for favorable conditions with $\epsilon = 1$, convergence was achieved for $\max(\tau_s) = 0.1$ after $N \sim 100$ species, but for $\max(\tau_s) = 1$ the timescale for the growth of the unstable mode is linearly increasing with the number of species, and does not seem to converge (see Figures 2 and 4 of Krapp et al. 2019).

By truncating the maximal range of τ_s to $\tau_\star$, the SI mechanism can achieve convergence. Convergence is typically achieved for $\max \tau_s \lesssim 0.1$. Thus, the SI is favorable in areas in the disk for which $\tau_\star \lesssim 0.1$, which we find to be the regions inward to $\sim$1 au, pending on dust size, disk model, and turbulence levels. The boundaries of these areas, where $\tau_\star \approx 0.1$, could therefore be the most favorable areas for SI, since this is the optimal Stokes number at which SI is effective with the lowest possible metallicity $Z \approx 0.03$, as shown in Yang et al. (2017).

Pebble accretion: SI is a growth mechanism for the first planetesimals. Once planetary cores of $\gtrsim 10^{2-3}$ km are formed, further growth is proceeded by accretion of pebbles until a critical core mass is reached, where runaway gas accretion begins leading to gas/ice giant formation. The efficiency of pebble accretion depends on their coupling to the gas, i.e., their Stokes number. Pebbles with $\tau_s \lesssim 10^{-3}$ are well coupled to the gas flow and unaffected by the core. Pebbles with $10^{-3} \leqslant \tau_s \leqslant 0.1$ are affected by the core's gravity, but contribute less to the overall collisions and accretion rates (Lambrechts & Johansen 2012). Pebbles with $\tau_s \gtrsim 0.1$ are accreted onto the protoplanet when the impact parameter is within the Hill-sphere. Pebbles with $\tau_s \approx 1$ are attracted from wider distances, but the horseshoe orbits with small impact parameters are lost (see Figure 7 of Lambrechts & Johansen 2012). The overall accretion rates are faster for Stokes numbers in the range of $0.1 \lesssim \tau_s \lesssim 1$, for large enough protoplanetary core of 10^3 km as seen, e.g., in Figure 10 of Ormel & Klahr (2010).

The radial erosion-induced stratification of dust sizes plays a similar role in the efficiency of pebble accretion. Similarly to SI, there are favorable regions in the disk where the critical Stokes number is around $\tau_\star \approx 0.1$–1, where pebble accretion is most probable. Since these are generally regions close to 1 au and inwards, the accreting cores are unlikely to form gas giants. Only for boulders composed of relatively large dust grains of $d \approx 1$ cm, could erosion be effective up to larger distances of $\sim$7 au, which is compatible with the formation locations of ice/giant planets. Evolved disks have lower densities (therefore, less erosive), and even larger grain composition (or closer separation) is required to be effective.

Caveats: In the derivation of Equations (6) and (8) we used dimensionless quantities. In reality, there are limitations to the smallest Stokes number available. The Stokes number is defined as $\tau_s \equiv (\pi/2)\rho_p d/\Sigma_g$. For our disk models, it is roughly $\tau_s \sim 10^{-3}(d/\mathrm{cm})(a/\mathrm{au})^{3/2}$. Thus, for the size of $d = 1$ cm the minimal Stokes is $\sim 10^{-3}$, which increases to $\sim$0.02 at $a \approx 7$ au. Obviously, the erosion cannot grind down boulders to sizes smaller than the fundamental composing-grain size, d; therefore, there is a physical limitation on the minimal Stokes number in our formalism.

Growing boulders and planetesimals can be porous and have various sizes and different densities and cohesive forces. From Equation (1) it is evident that detaching larger grains is easier than smaller ones. Thus, if an eroding object is composed of grains of various sizes, only grains above some threshold can be detached, which will affect the structure of the growing boulders and requires further study.

The erosion timescales are usually shorter than the radial drift times, but the drift itself is much faster than the disk's lifetime. As the particle will drift inward, its critical Stokes number will keep decreasing due to the decrease of the threshold velocity. Obviously, with no drift stopping mechanism, the body will be lost. Nevertheless, even if the body is lost, some of the fractions of the detached grains during the erosion process may survive and serve as reservoirs for the later growth mechanisms.

It is also tempting to apply our formalism for large pebbles of sizes $\sim$10 cm, since they are more favorable to efficient erosion. However, the aeolian-erosion formalism is relying on the assumption that the cohesive forces are linearly proportional to the dust grain size d. The proportionality constant was derived experimentally for small grain sizes of μ-size. We extrapolated the linear behavior up to $\lesssim$0.1 cm pebbles in Rozner et al. (2020), largely based on laboratory experiments of Paraskov et al. (2006) for 0.05 cm size grains, which seem to be consistent with our derived erosion rates. It is unclear if the linear proportionality could be extended beyond 1 cm scale. On the other hand, erosion of smaller grains from the surface may destabilize and weaken the cohesion of larger grains, possibly attached through contact with smaller grains. In this case erosion might be even more efficient. More generally, the nature of the forces that bring together the planetesimals that are composed of pebbles could be different and depend on the composition, porosity, and equation of state, as well as self-gravity for the larger objects. We therefore caution using our model to larger dust/pebble sized and defer it to future studies.

4. Summary

In this Letter we showcased that aeolian-erosion can efficiently grind down solids in protoplanetary disks into smaller grains/pebbles down to the point where they are coupled to the gas flow. The strength of the coupling is measured by the critical Stokes number $\tau_\star$ (Equations (6), (8)), which in turn depends on the ratio of the threshold velocity $v_{\rm th}$ (Equation (1)) and the typical relative laminar and turbulent velocities, and on the size of the detaching grains/pebbles d.

The dependence can be related to the radial location on the disk (Figure 2), and the general trend is that $\tau_\star$ is decreasing with decreasing radial location, until some critical separation where aeolian-erosion becomes inefficient.

Growth of planetesimals due to the streaming instability and the growth of planetary cores due to pebble accretion rely on large numbers of pebbles with "optimal" Stokes numbers with nontrivial coupling with the gas. A wide size-distribution of small particles slows down the growth, since fewer particles participate, and complex coupling between different sizes may play a role and hinder the growth; therefore, simplified assumptions in modeling of these processes through the use of ubiquitous, mono-sized pebbles is heavily criticized. However, as we show here, aeolian-erosion processes naturally produce particle sizes of typical Stokes number, depending on the radial separation. Erosion may therefore allow for a realistic, naturally produced limited pebble-size range. Optimal Stokes numbers are a natural consequence and are expected to then be present at preferred locations. The critical Stokes numbers depend not only on locations but also on time. Evaporating disks with lower gas density increase the critical Stokes number with time. Therefore, depleted disks (at later times or with local cavities) are better sites for planet/planetesimal formation mechanisms that require nontrivial coupling (e.g., $\tau_\star \approx 0.1$–1) of gas and dust, such as the streaming instability or pebble accretion.

We thank Jake Simon, Allona Vazan, Andrew Youdin, and Yanqin Wu for useful discussions. E.G. and M.R. acknowledge useful discussions at the Rocky Worlds workshop at the KICC, which initiated this work. H.B.P. acknowledges support from the MINERVA center for "Life under extreme planetary conditions" and the Kingsley fellowship at Caltech.

ORCID iDs

Evgeni Grishin https://orcid.org/0000-0001-7113-723X
Hagai B. Perets https://orcid.org/0000-0002-5004-199X

References

Abel, N. H. 1824, Œuvres Complètes de Niels Henrik Abel (in French) (2nd ed.; Oslo: Grøndahl & Søn), 28
Adachi, I., Hayashi, C., & Nakazawa, K. 1976, PThPh, 56, 1756
Andersen, M., Steinacker, J., Thi, W. F., et al. 2013, A&A, 559, A60
Armitage, P. J. 2010, Astrophysics of Planet Formation (Cambridge: Cambridge Univ. Press)
Bai, X.-N., & Stone, J. M. 2010, ApJL, 722, L220
Banzatti, A., Testi, L., Isella, A., et al. 2011, A&A, 525, A12
Barge, P., & Sommeria, J. 1995, A&A, 295, L1
Benítez-Llambay, P., & Pessah, M. E. 2018, ApJL, 855, L28
Bitsch, B., Lambrechts, M., & Johansen, A. 2015, A&A, 582, A112
Blum, J., & Wurm, G. 2008, ARA&A, 46, 21
Brouwers, M. G., Vazan, A., & Ormel, C. W. 2018, A&A, 611, A65
Carrera, D., Gorti, U., Johansen, A., & Davies, M. B. 2017, ApJ, 839, 16
Chen, J.-W., & Lin, M.-K. 2018, MNRAS, 478, 2737
Chiang, E., & Youdin, A. N. 2010, AREPS, 38, 493
Chiang, E. I., & Goldreich, P. 1997, ApJ, 490, 368
Demirci, T., Schneider, N., Steinpilz, T., et al. 2020, MNRAS, 493, 5456
Galois, E. 1846, J. Math. Pures Appl., 11, 417
Grishin, E., & Perets, H. B. 2015, ApJ, 811, 54
Grishin, E., Perets, H. B., & Avni, Y. 2019, MNRAS, 487, 3324
Hayashi, C. 1981, PThPS, 70, 35
Iversen, J. D., & White, B. R. 1982, Sedim, 29, 111
Jin, S., Isella, A., Huang, P., et al. 2019, ApJ, 881, 108
Johansen, A., Youdin, A., & Klahr, H. 2009a, ApJ, 697, 1269
Johansen, A., Youdin, A., & Mac Low, M.-M. 2009b, ApJL, 704, L75
Krapp, L., Benítez-Llambay, P., Gressel, O., & Pessah, M. E. 2019, ApJL, 878, L30
Lambrechts, M., & Johansen, A. 2012, A&A, 544, A32
Lambrechts, M., & Lega, E. 2017, A&A, 606, A146
Lee, E. J., & Chiang, E. 2016, ApJ, 817, 90
Li, R., Youdin, A. N., & Simon, J. B. 2019, ApJ, 885, 69
Liu, B., Ormel, C. W., & Johansen, A. 2019, A&A, 624, A114
Mamajek, E. E. 2009, in AIP Conf. Ser. 1158, Exoplanets and Disks: Their Formation and Diversity, ed. T. Usuda, M. Tamura, & M. Ishii (Melville, NY: AIP), 3
Mathis, J. S., Rumpl, W., & Nordsieck, K. H. 1977, ApJ, 217, 425
Menu, J., van Boekel, R., Henning, T., et al. 2014, A&A, 564, A93
Morbidelli, A., Bottke, W. F., Nesvorný, D., & Levison, H. F. 2009, Icar, 204, 558
Nesvorný, D., Li, R., Youdin, A. N., Simon, J. B., & Grundy, W. M. 2019, NatAs, 3, 808
Nesvorný, D., Youdin, A. N., & Richardson, D. C. 2010, AJ, 140, 785
Ormel, C. W., & Klahr, H. H. 2010, A&A, 520, A43
Ormel, C. W., & Liu, B. 2018, A&A, 615, A178
Pagani, L., Steinacker, J., Bacmann, A., Stutz, A., & Henning, T. 2010, Sci, 329, 1622
Paraskov, G. B., Wurm, G., & Krauss, O. 2006, ApJ, 648, 1219
Perets, H. B., & Murray-Clay, R. A. 2011, ApJ, 733, 56
Pfalzner, S., & Bannister, M. T. 2019, ApJL, 874, L34
Pinilla, P., Birnstiel, T., Ricci, L., et al. 2012, A&A, 538, A114
Pollack, J. B., Hubickyj, O., Bodenheimer, P., et al. 1996, Icar, 124, 62
Raettig, N., Klahr, H., & Lyra, W. 2015, ApJ, 804, 35
Raymond, S. N., & Cossou, C. 2014, MNRAS, 440, L11
Rosenthal, M. M., & Murray-Clay, R. A. 2018, ApJ, 864, 66
Rosenthal, M. M., & Murray-Clay, R. A. 2019, arXiv:1908.06991
Rosenthal, M. M., Murray-Clay, R. A., Perets, H. B., & Wolansky, N. 2018, ApJ, 861, 74
Rozner, M., Grishin, E., & Perets, H. B. 2020, MNRAS, 496, 4827
Ruffini, P. 1799, Teoria Generale delle Equazioni, Parte Prima (in Italian) (Bologna: Nella Stamperia di S. Tommaso D'Aquino)
Schaffer, N., Yang, C.-C., & Johansen, A. 2018, A&A, 618, A75
Sekiya, M., & Onishi, I. K. 2018, ApJ, 860, 140
Shao, Y., & Lu, H. 2000, JGR, 105, 437
van Boekel, R., Henning, T., Menu, J., et al. 2017, ApJ, 837, 132
Visser, R. G., & Ormel, C. W. 2016, A&A, 586, A66
Weidenschilling, S. J. 1977, MNRAS, 180, 57
Yang, C. C., Johansen, A., & Carrera, D. 2017, A&A, 606, A80
Youdin, A. N., & Goodman, J. 2005, ApJ, 620, 459
Zhu, Z., Nelson, R. P., Dong, R., Espaillat, C., & Hartmann, L. 2012, ApJ, 755, 6